THE JOURNAL OF PHYSICAL CHEMISTRY C
A JOURNAL OF THE AMERICAN CHEMICAL SOCIETY

pubs.acs.org/JPCC

Article

Operando Investigations of the Interfacial Electrochemical Kinetics of Metallic Lithium Anodes via Temperature-Dependent Electrochemical Impedance Spectroscopy

Mohammed Ahmed Zabara, Gökberk Katırcı, and Burak Ülgüt*

Cite This: *J. Phys. Chem. C* 2022, 126, 10968−10976

Read Online

ACCESS | Metrics & More | Article Recommendations | Supporting Information

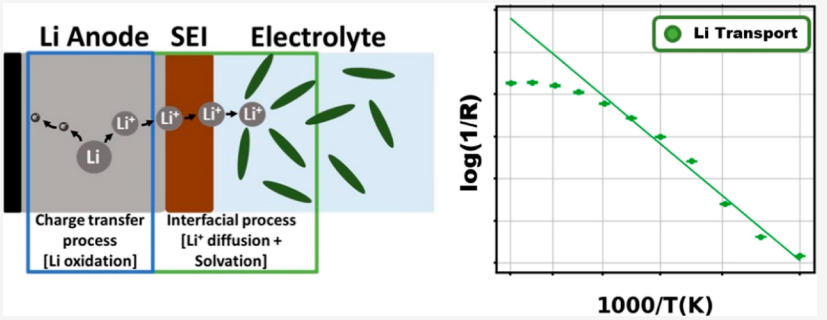

ABSTRACT: One of the major hurdles in the utilization of metallic lithium anodes is understanding the Li^+ transfer kinetics through the solid electrolyte interface (SEI) in addition to Li oxidation. Electrochemical impedance spectroscopy (EIS) combined with temperature variation provides deeper comprehension and reveals kinetic parameters of individual processes separately. In this study, we report temperature-dependent EIS analysis of metallic Li anodes to shed light on the kinetics of anodic/interfacial processes at different states of charge and wide temperature ranges (−25 to 75 °C), utilizing lithium thionyl chloride ($Li/SOCl_2$) and lithium manganese dioxide (Li/MnO_2) primary batteries as model systems. We found in both batteries that the impedance of the SEI processes is highly temperature-dependent with non-Arrhenius behavior at temperatures greater than 35 °C. Conversely, the kinetics of the anodic process showed small temperature dependence that is explained by the Arrhenius equation throughout the temperature range studied. The results provide a deeper understanding of the underlying processes separately in metallic Li anodes under operando and real-time conditions.

INTRODUCTION

Lithium batteries (LBs) with metallic lithium (Li) anodes provide higher gravimetric and volumetric energy densities than intercalation-based anodes. Such batteries are already commercially available as non-rechargeable (primary), which are heavily used in applications where charging is impractical or impossible.[1−3] The limitations hindering the use of metallic Li anodes in rechargeable batteries are in the charging process with mainly inhomogeneous Li electrodeposition (mossy and/or dendritic),[4−8] which leads to performance limitations and safety concerns. In recent years, many studies have been done to investigate these processes deeply, with the aim of finding solutions that limit those setbacks and achieve optimized operating conditions for rechargeable LBs employing metallic Li anodes.[9−15]

Electrochemical impedance spectroscopy (EIS) is one of the most-used techniques for characterizing the different electrochemical processes in batteries in general and LBs in particular. Its in situ and noninvasive nature is the most attractive property for LB research, which should be performed in a sealed inert environment. It has proven its usefulness for different LB variants by providing electrochemical parameters regarding Li charge and mass transfer in active materials, electrolytes, and the formed interfaces independently from each other.[16−20] Furthermore, it is utilized as a probe for state-of-health and state-of-charge (SoC) determination, and for modeling the voltage response of the LBs.[21−24] Lastly, it represents a powerful tool to study the electrochemical processes taking place during the operation of the battery and to determine the limiting factors affecting the process.[25,26]

EIS is most useful when coupled with variations in the studied system parameters. In LBs, EIS studies are conducted with variations in the composition/amount of the active materials or the electrolytes to investigate the change in the

Received: April 8, 2022
Revised: June 15, 2022
Published: June 28, 2022

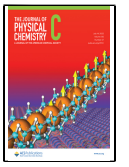

impedance response, which corresponds to the change in the underlying processes. This has been shown to be very useful not only in matching the portion of the impedance response to the corresponding electrochemical process but also in finding the best amount and composition of material for better battery performance.[27−30]

Temperature variation has a high impact on the electrochemical processes of the LBs.[31] The resistance involved in the charge and the mass transfer processes, in addition to the electrolyte conductivity, are dependent on the temperature of the system. Investigating the temperature dependence provides insight into the dominant electrochemical processes at the operating temperature of the battery.[32,33] Moreover, it can be used to extract kinetic and thermodynamic properties of the electrochemical processes by employing temperature (T)-dependent equations, such as the Arrhenius relation.[34−36]

Li^+ transport through the solid electrolyte interface (SEI) on the graphite anode is deeply investigated for Li-ion intercalation chemistries.[37−40] The underlying processes are assigned as Li^+ diffusion through the solid-state SEI followed by the solvation process before the ion diffuses out into the electrolyte.[38,41] The contribution of each process is still under active research with several findings suggesting the differences are due to the type of electrolyte, which directly affects the structure and composition of the formed SEI.[34,39,40,42−45] These processes are presumably similar in metallic Li anodes; however, structure and properties of the SEI will clearly be different. To the best of our knowledge, this manuscript is the first to report on the properties of the SEI formed on the surface of the metallic lithium through the T-dependence of the electrochemical impedance response resolving the details of underlying processes.

In this study, aiming to better understand the anodic/interfacial processes in LBs with metallic Li anodes, we investigate T-dependent EIS for two different Li primary battery chemistries which use metallic Li as their anode. The first is lithium thionyl chloride ($Li/SOCl_2$) and the second is lithium manganese dioxide (Li/MnO_2). We use these commercial cells because they provide the most reproducible results as they are mass-produced. Through equivalent circuit (EC) fits for the obtained impedance, we report, for the first time, calculated activation energies of the process of Li^+ transport through the SEI of the metallic Li anode in addition to the oxidation of the metal to the cation. The variation of the obtained activation energies for the various processes as the SoC changes is investigated to understand better operation conditions.

EXPERIMENTAL SECTION

T-dependent EIS was performed in a wide temperature range (−25 to 75 °C), with 10 °C increments. The T-dependent EIS measurements were repeated with at least three cells of the same chemistry to ensure the reproducibility of the data.

Cells. $Li/SOCl_2$ (SAFT- LS 14500) AA-size cell with 2.6 Ah capacity and 3.67 V open circuit potential and Li/MnO_2 (Panasonic LM2023) coin cell with 2 mA h capacity and 3.20 V open circuit potential were used.

Temperature Control. The T-dependent EIS experiments were performed in a temperature range from −25 to 75 °C. The temperature was measured using a thermocouple which was placed in a custom-made insulating chamber. A thermoelectric cooler (Peltier device) was placed on one side of the chamber to provide the required cooling. The Peltier device was able to cool the temperature to 5 °C. Further cooling was done by placing a beaker filled with liquid Nitrogen, where the temperature was controlled manually. Higher temperatures (25−65 °C) were achieved by placing heating stripes, in which the heating was controlled by controlling the voltage source. At higher temperatures, the temperature inside the chamber was stabilized by the Peltier device.

The studied cells were placed inside the chamber before the EIS experiments, which were also connected to the Gamry 5000E instrument. EIS measurements were performed after bringing the chamber's temperature to the desired value and waiting at that temperature for at least 10 min prior to the measurement. Consecutive EIS measurements confirmed that 10 min was enough for the cell to stabilize at the chamber's temperature (i.e., <1% variation).

EIS Measurement. Galvanostatic-EIS at discharge was performed for the cells by applying a negative DC offset along with the AC excitation. For $Li/SOCl_2$ −10 mA DC offset was applied along 2 mA ACamplitude for a frequency range of 1 MHz to 100 mHz. For Li/MnO_2 −3 mA DC offset was applied along 2 mA AC amplitude for a frequency range of 1 MHz to 1 Hz. These values were chosen by prior trial-and-error measurements along with Kramers−Kronig compatibility tests for the best parameters.

Kramers−Kronig Compatibility Test. All obtained EIS data were validated with the Kramers−Kronig compatibility test to check for the presence of nonlinearity and instability. Gamry Echem Analyst Software's (v.7.8.5) Kramers−Kronig tool was used for testing the data. The observed compatibility is overlayed with the data in the Nyquist plots presented throughout the manuscript.

SoC Measurements. The SoC was determined by coulomb counting. Fresh cells were assigned as 100% SoC and were discharged after the EIS measurements for a certain amount of time. The discharge current was −10 mA for the $Li/SOCl_2$ battery and −3 mA for the Li/MnO_2 battery. The percentages were calculated as a fraction of the labeled capacities.

Arrhenius Analysis. The T-dependence is investigated by extracting charge transfer resistance values from the impedance response, with the aid of EC fits and by observing the change with respect to the temperature change. The obtained charge transfer resistances are related to the activation energy of the electrochemical process through the Arrhenius equation

$$k = Ae^{-E_a/RT} \propto \frac{1}{R_{CT}} \tag{1}$$

where k is the rate constant of the electrochemical process, R_{CT} is the charge transfer resistance, A is the pre-exponential factor, E_a is the activation energy, R is the gas constant, and T is the temperature.

To obtain the activation energy, typically, a plot of the rate constant as a function of $1000/T$ is used. The form of the Arrhenius equation that justifies this use is the logarithmic form that can be written as

$$\log k = \log A - \frac{E_a\left(\text{in}\frac{\text{J}}{\text{mol}}\right)}{R} \bullet \frac{1}{T} \tag{2}$$

or

https://doi.org/10.1021/acs.jpcc.2c02396
J. Phys. Chem. C 2022, 126, 10968−10976

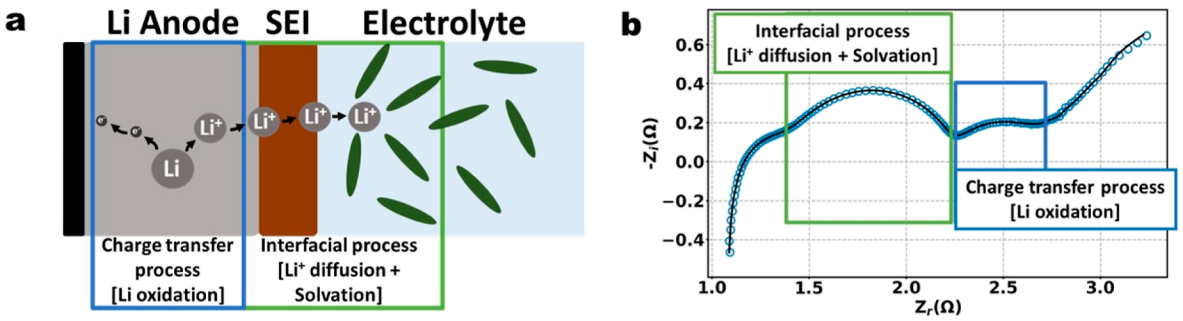

Figure 1. (a) Electrochemical processes of the metallic Lithium anodes are mainly related to the oxidation of the Li followed by the transfer and solvation of Li^+ to the electrolyte, (b) Nyquist plot related to the electrochemical processes of the metallic Li anode.

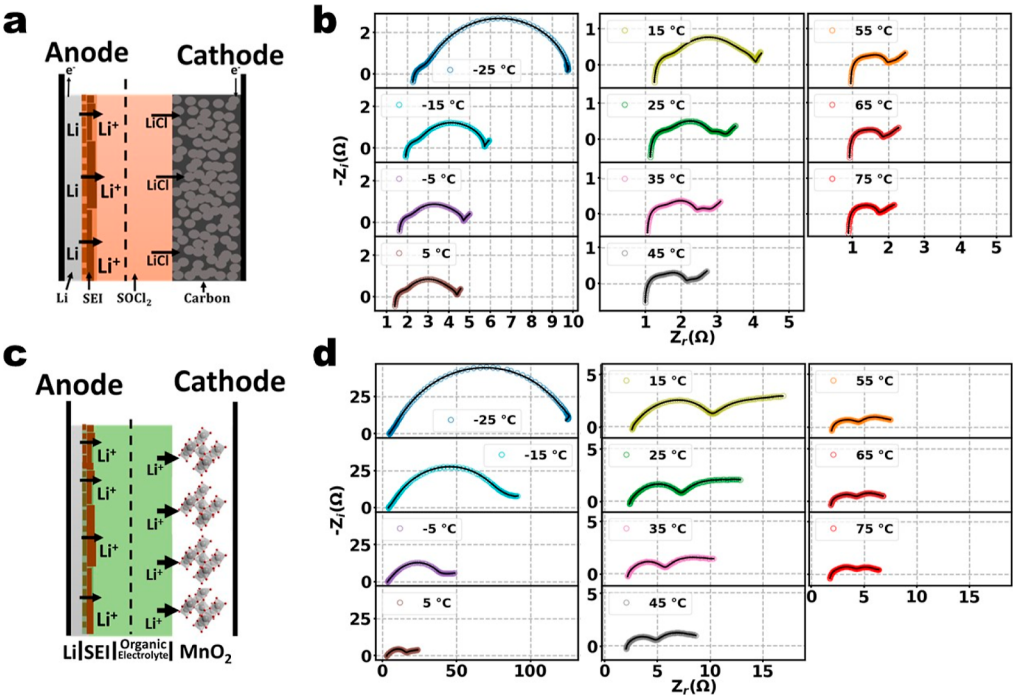

Figure 2. Schematic representation of the structure and the movement of Li^+ for (a) lithium thionyl chloride ($Li/SOCl_2$) and (c) lithium manganese dioxide (Li/MnO_2); Nyquist plots of temperature-dependent EIS from 1 MHz to 100 mHz at 90% SoC for (b) $Li/SOCl_2$ and (d) Li/MnO_2, the overlayed black lines are the results of the Kramers−Kronig compatibility test.

$$\log k = \log A - \frac{E_a\left(\text{in}\frac{\text{kJ}}{\text{mol}}\right)}{R} \bullet \frac{1000}{T} \tag{3}$$

When using the inverse of the parallel resistances as proxies for the rate constants, the additional terms that are required to convert the resistance to the rate constant have to be considered.

$$\log \frac{c}{R} = \log A - \frac{E_a\left(\text{in}\frac{\text{kJ}}{\text{mol}}\right)}{R} \bullet \frac{1000}{T} \tag{4}$$

where c is the collective multiplier that is required to convert the measured resistance to a rate constant. This equation simplifies to

$$\log \frac{1}{R} = \log A - \log c - \frac{E_a\left(\text{in}\frac{\text{kJ}}{\text{mol}}\right)}{R} \bullet \frac{1000}{T} \tag{5}$$

As can be seen, in a plot of $\log 1/R$ versus $1000/T$, the additional terms appear in the intercept and do not change the slope at all. It is important to note that the collective multiplier c includes any corrections that are associated with the different electroactive areas of the various electrodes. Therefore, the numbers obtained from AA and button size batteries are perfectly comparable, because any difference that is related to the difference in electrode areas will be observed in the intercept and will not affect the slopes.

RESULTS AND DISCUSSION

The EIS of LBs provides information about the redox and the interfacial processes in the metallic Li anode in addition to others. Several semicircles in the Nyquist plot represent various processes in the impedance response, according to their timescales. Several experimental and computational studies assigned the electrochemical processes to their corresponding frequency regions in the impedance response. For almost all LBs, the impedance response at high frequencies (100 kHz to 100 Hz) is assigned to the interfacial processes, which results from the movement of the Li^+ ions through the SEI. The anodic Faradaic processes show impedance response in the

https://doi.org/10.1021/acs.jpcc.2c02396
J. Phys. Chem. C 2022, 126, 10968−10976

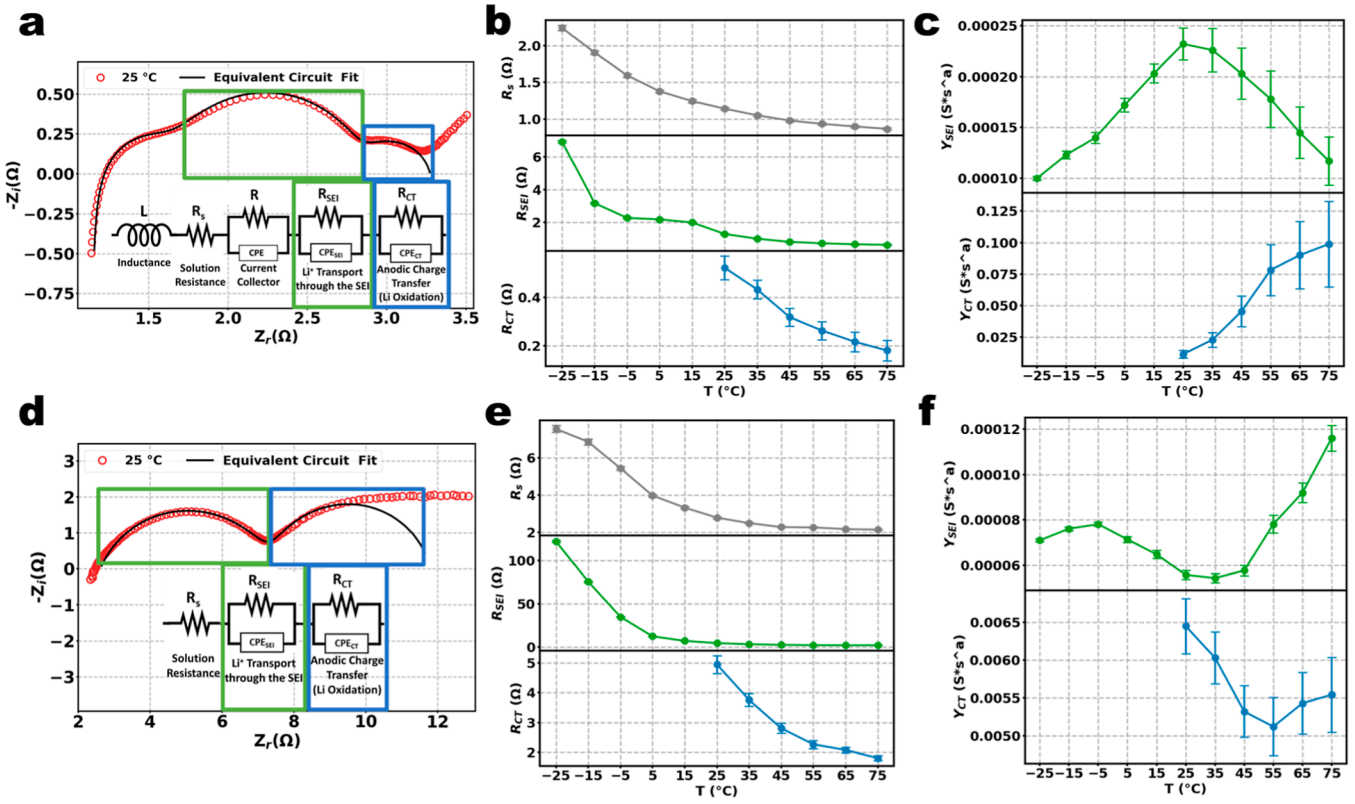

Figure 3. Fitted EC model overlayed with the Nyquist plot for 90% SoC (a) Li/$SOCl_2$ and (d) Li/MnO_2, *R* and *Y* values obtained from EC parameters for (b,c) Li/$SOCl_2$ and (e,f) Li/MnO_2 batteries.

medium frequency regions (100 Hz to 100 mHz), whereas at lower frequencies, cathodic and mass transfer processes are known to appear.[46−48]

The impedance response is the result of Li^+ movements through the SEI toward the electrolyte after oxidation at the surface. This movement takes place in two consecutive processes, which is illustrated in Figure 1a. First Li^+ diffuses through the solid-state SEI then there is solvation of Li^+ into the electrolyte.[38,40,42] The contribution of each process is still a topic of active research, yet clearly dependent on the chemistry of the LB and is characteristic to the type and composition of the electrolyte used.[34,37,43,49] The obtained EIS response for these processes is observed in two successive semicircles in the Nyquist plot as shown in Figure 1b.

Temperature-Dependent EIS. The *T*-dependence of EIS response is observed to be large for the Li anode processes, which can be seen in Figure 2. The result shows an overlay of *T*-dependent EIS data validated with the Kramers−Kronig compatibility test. The Kramers−Kronig test is vital to demonstrate the linearity and stability of the obtained data, which will be analyzed to characterize electrochemical processes at the Li anode.[50,51]

The investigated batteries both utilize Li metal as their anode active material. They differ in the type of electrolyte and cathode active material. As can be seen in Figure 2a,c, Li/$SOCl_2$ uses $SOCl_2$ with dissolved $LiAlCl_4$ as the electrolyte, whereas Li/MnO_2 uses $LiClO_4$ dissolved in Propylene Carbonate and Dimethoxyethane as electrolyte. Moreover, Li/$SOCl_2$ has porous carbon as the cathode surface, while Li/MnO_2 used MnO_2 as the host for the Li^+ ions. Although they have different electrolytes and cathode active materials, their EIS responses are similar at high- and middle-frequency regions, further evidence that anodic processes are observed at these frequency ranges, see Figure 2b,d.

Nyquist plots for the *T*-dependent EIS for both Li/$SOCl_2$ and Li/MnO_2 for a temperature range of −25 to 75 °C are shown in Figure 2b,d, Bode plots can be found in the Supporting Information. In both chemistries, two semicircles are observed which are *T*-dependent, the first in the high-frequency range (100 kHz to 100 Hz) and the second in the middle frequency range (100 Hz to 100 mHz).[a] Both semicircles are observed for temperatures above 15 °C. Below this temperature, the high-frequency semicircle dominates the EIS response with large impedance values. The first semicircle is assigned to the SEI processes and the second to Li oxidation. The domination in the SEI impedance for below 15C temperatures is related to the slow kinetics of the Li^+ mass transport through the SEI.

As can be observed from the Nyquist plots in Figure 2, there is a drastic decrease in the size of the first semicircle as the temperature increases from −25 to 35 °C, which then continues to decrease at a lower rate from 35 °C to 75 °C. The second semicircle shows a small decrease as the temperature rises from 25 °C to 75 °C. This variation can be correlated to the nature of processes for each semicircle, the first for the mass transfer of Li^+ through the SEI and the second for the oxidation of Li.

EC Fits. In order to perform the Arrhenius analysis on the charge transfer resistances for the two semicircles obtained, we extracted the resistance values through EC fit. The fitted circuits for each battery are shown in Figure 3a,d. For each semicircle, a charge transfer resistance in parallel connection to a constant phase element (CPE) was used. As can be noticed, Li/$SOCl_2$ EIS contained inductive and *T*-independent semi-

https://doi.org/10.1021/acs.jpcc.2c02396
J. Phys. Chem. C 2022, 126, 10968−10976

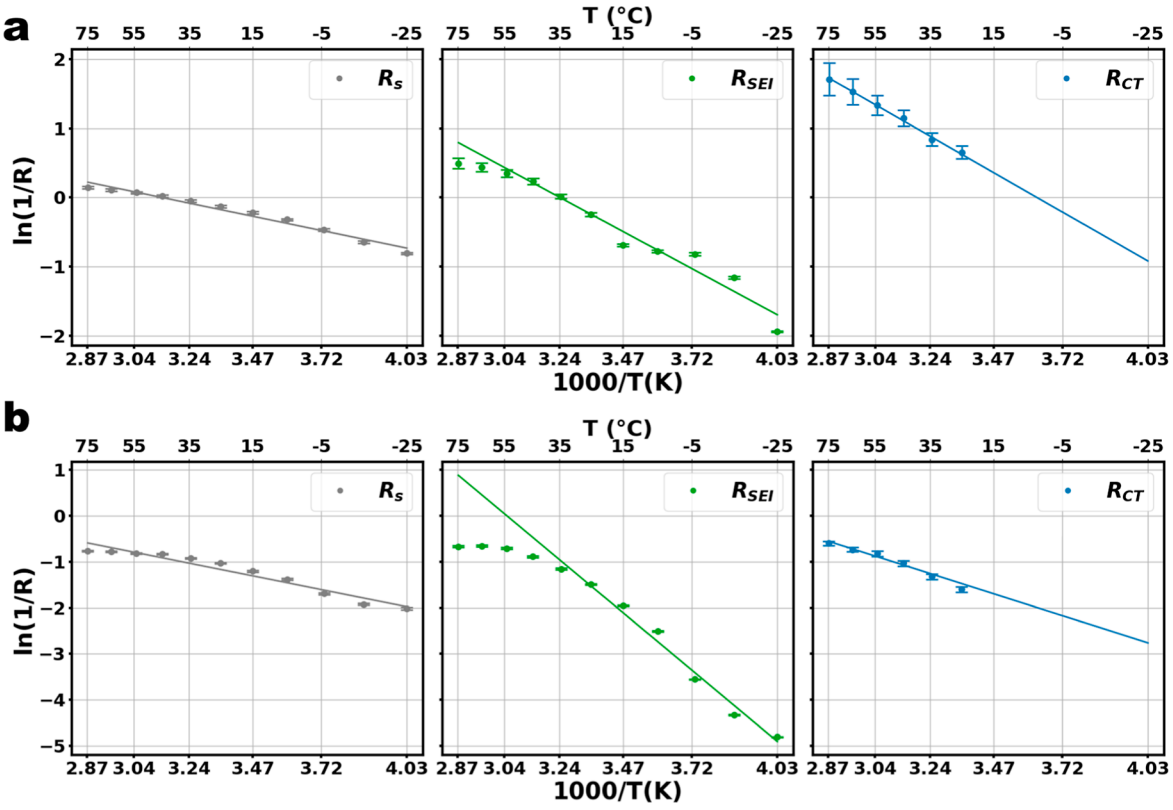

Figure 4. Arrhenius plots for resistance values (R_s, R_{SEI}, R_{CT}) for 90% SoC of (a) lithium thionyl chloride ($Li/SOCl_2$) and (b) lithium manganese dioxide (Li/MnO_2).

circle at very high frequencies, (1 MHz to 100 kHz) which was fitted and not taken for analysis.

The parameters obtained along with the respective errors are demonstrated in Figure 3. The three resistances obtained from the EC fits are electrolyte resistance (R_s), interfacial resistance (R_{SEI}), and anodic charge transfer resistance (R_{CT}). Figure 3b,e shows the trends in the obtained resistances with increasing temperature for $Li/SOCl_2$ and Li/MnO_2 respectively. The two corresponding Y_0 values from the CPEs are shown in Figure 3c,f. It can be seen from the trends that, while all the resistances show a decrease as the temperature rises, the interfacial resistance R_{SEI} shows the sharpest decrease in its value, especially at low temperatures. There is a measurable change in the fitted CPE parameters, namely Y_{SEI} and Y_{CT} values as the temperature changes, even though the degree of variations is small. However, this change is not showing clear T-dependence. The reasons and the information content of Y values require further investigation and are beyond the scope of this manuscript.

Arrhenius Analysis. Arrhenius plots using the obtained resistance values exhibit linearity with all the resistances, which can be seen in Figure 4. However, for the interfacial resistance R_{SEI}, there is a deviation from the Arrhenius relation at temperatures higher than 35 °C. This is observed in both batteries indicating that the charge transfer of Li^+ movement through the SEI plus solvation involves both Arrhenius and non-Arrhenius behavior, depending on the operating temperature of the battery. This indicates that after 35 °C, the combination of Li^+ diffusion through the SEI plus solvation occurs through a mechanism that is not thermally activated. Therefore, increasing the temperature to a higher degree will not increase the kinetics of this process.

Observing the identical non-Arrhenius behavior shows the similarity in Li^+ formation and transport mechanism for both batteries. Although the electrolytes and consequently structure and composition of the SEI are different, the transition from a thermally activated mechanism to one that is not affected by temperature occurs around the same levels. This non-Arrhenius behavior is also reported for Li-ion batteries with graphite anodes[52,53] and was investigated for its effect on the fast charging protocols.[54] The behavior was related to the diffusion of Li^+ in different phases of graphite. Detecting the same deviation from Arrhenius behavior for Li^+ transport in nonintercalation chemistry raises several questions about its diffusive and solvation processes and calls for further fundamental mechanistic investigation at these temperature ranges.

Activation energies (E_a) calculated are summarized in Table 1. As can be seen, the activation energies for the anodic charge transfer (Li oxidation) in both cells show similar values. The activation energy for the charge transfer resistance for lithium oxidation at high SoCs is calculated to be around 20 kJ/mol, which is in accordance with reported values for the same process in intercalation chemistries.[55−57] The fact that this number is very close in both chemistries is a clear indication that this process is very similar in both. Though for 100% SoC in $Li/SOCl_2$, the calculated energies are lower which is related to the high amount of the solvent $SOCl_2$ which is also the cathode active material, and the undeveloped structure of the SEI.

However, the values of the activation energies for the transport through the SEI processes differ. Li/MnO_2 has roughly double the activation energy with ≈40 kJ/mol compared to ≈20 kJ/mol for $Li/SOCl_2$. This change can be

https://doi.org/10.1021/acs.jpcc.2c02396
J. Phys. Chem. C 2022, 126, 10968−10976

Table 1. Calculated Activation Energies Obtained from the Arrhenius Plots of the Resistances for the Two Batteries at Different % States-of Charge

		E_a for		
	% SoC	R_s (kJ/mol)	R_{SEI} (kJ/mol)	R_{CT} (kJ/mol)
$Li/SOCl_2$	100	2.95 ± 0.39	10.16 ± 1.39	3.17 ± 0.47
	90	6.65 ± 0.61	17.88 ± 3.64	18.63 ± 0.49
	70	7.12 ± 0.34	21.37 ± 2.23	21.06 ± 0.66
	50	5.30 ± 0.51	27.44 ± 2.15	15.44 ± 0.75
	40	5.89 ± 0.91	31.54 ± 5.22	12.38 ± 0.91
Li/MnO_2	100	10.43 ± 3.48	44.96 ± 3.86	17.45 ± 0.33
	90	8.92 ± 2.48	41.19 ± 3.49	17.44 ± 1.12
	70	9.02 ± 1.59	43.62 ± 2.85	22.57 ± 0.89
	50	9.22 ± 1.72	40.18 ± 3.04	19.90 ± 1.05
	30	10.33 ± 2.23	39.26 ± 2.35	19.17 ± 0.86
	10	14.63 ± 4.17	37.14 ± 1.88	10.83 ± 1.12

related to the different structure and composition of the SEI and the type of electrolyte in both batteries. The SEI is the product of the reaction between Li and the components of the electrolytes. In graphite anodes, several studies suggest the formation of the mosaic structure of organic and inorganic Li-containing molecules.[41] In Li/MnO_2 the SEI possesses another complex structure as the result of the Li reaction with the various components of the electrolyte (propylene carbonate, dimethoxyethane plus $LiClO_4$).[58,59] The Li^+ transport through this layer is suggested to occur by pore diffusion and interstitial knock-off mechanisms[38,40] which are reported in the literature to have activation energy between 40 and 60 kJ/mol depending on the type of electrolyte.[34,37,39] In $Li/SOCl_2$, the SEI is shown to be mostly from LiCl crystals formed by the reaction of Li with $SOCl_2$ passivating the surface of the Li anode.[60] It is demonstrated that Li^+ is transported through the formed SEI by forming channels (cracks) that allow the ions to pass. This mechanism is also known to cause a voltage delay at the beginning of the operation.[61−63] Li^+ transport through the formed channels appears to require lower activation energy than the transport through the SEI of Li anodes with organic electrolytes such as Li/MnO_2.

Variation in SoC. Investigation of the Arrhenius relation for the obtained resistances was performed for the different SoC levels of both chemistries. Figure 5 shows the Arrhenius plots at different SoCs for the different processes. As can be noticed in all SoCs for both batteries, deviation from the Arrhenius relation for the SEI process is observed above 35 °C, indicating the existence of a nonthermally activated mechanism in all SoCs. Additionally, the slopes of the linear parts of the Arrhenius plots for $Li/SOCl_2$ show a steady increase as the SoC decreases, whereas Li/MnO_2 shows the opposite behavior.

The variation in the calculated activation energies is demonstrated in Figure 6a−c for R_s, R_{SEI}, and R_{CT} respectively, which are summarized in Table 1. The calculated activation energies for the SEI process in Li/MnO_2 appear to be roughly steady at around 40 kJ/mol, while $Li/SOCl_2$ shows an increase from 10 to 30 kJ/mol as the SoC decreases. This can be explained as mentioned above by the structure and composition of the SEI in each battery. While Li/MnO_2 possesses a stable structure with a complex composition that needs higher thermal activation, $Li/SOCl_2$ has a less stable and dynamic structure that continuously decomposes and forms via passivation reactions. Moreover, the increase in the Li^+ diffusion activation energy for $Li/SOCl_2$ is speculated to be from the depletion of the solvent $SOCl_2$, which is also the cathode active material. Decreasing solvent intuitively will hinder the Li^+ solvation process. The activation energy of lithium oxidation that is, R_{CT} increases initially as the state of

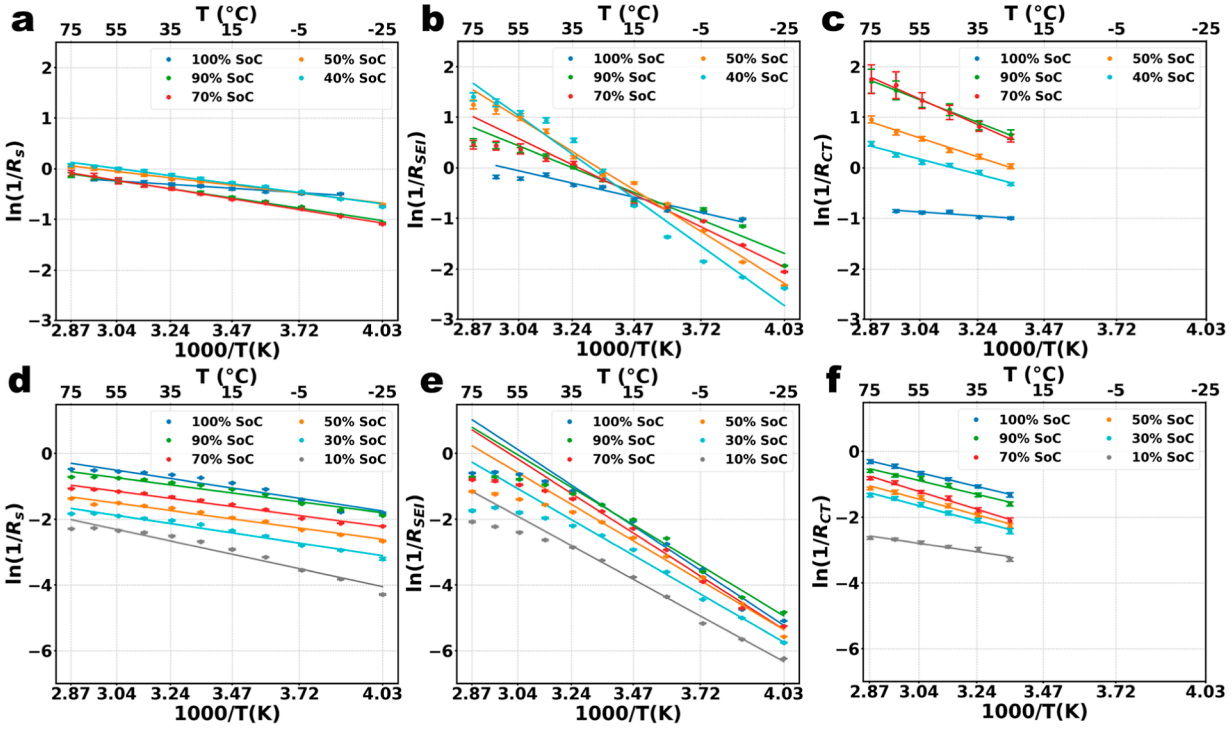

Figure 5. Arrhenius plots of R_s, R_{SEI}, and R_{CT} for different states-of-charge (SoC) for (a−c) lithium thionyl chloride ($Li/SOCl_2$) and (d−f) lithium manganese dioxide (Li/MnO_2).

https://doi.org/10.1021/acs.jpcc.2c02396
J. Phys. Chem. C 2022, 126, 10968−10976

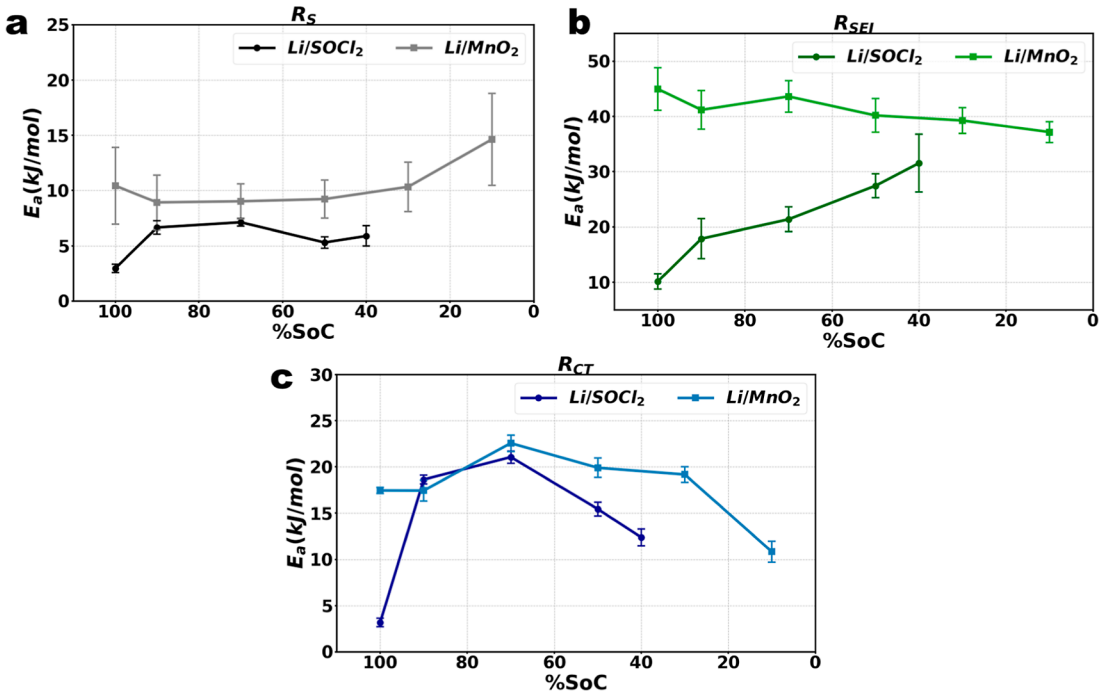

Figure 6. Change in activation energies with SoC for $Li/SOCl_2$ and Li/MnO_2 (a) R_s, (b) R_{SEI}, and (c) R_{CT}.

charge decreases, ultimately decreasing again at low states of charge. We speculate that the increase in the activation energy is related to the depletion of Li and the decrease is related to an increase in the effective electrode area, as the surface gets rougher at lower states of charge.

CONCLUSIONS

In summary, we have shown that T-dependent EIS is a valuable tool to investigate the kinetics of Li^+ diffusion across the SEI and oxidation of metallic lithium to form Li^+. The study was performed on two different battery chemistries by investigating the *T*-dependence of the parallel resistances of the semicircles representing Li^+ transport across the SEI and Li oxidation. Ultimately, activation energies were calculated for these processes. High *T*-dependence was observed for the transport of Li^+ ions across the SEI with *T*-independent transport above a certain temperature, indicating a transition to a nonthermally activated mechanism, which calls for further investigation. In both batteries, the activation energies for the Li oxidation showed similar values but varied for the transport through the SEI. The variation was related to the structure and composition of the formed SEI in the two chemistries. These findings demonstrate the power of *T*-dependent EIS in elucidating the kinetics that the metallic Li anode processes and highlight its usefulness in understanding the underlying processes.

ASSOCIATED CONTENT

Supporting Information

The Supporting Information is available free of charge at https://pubs.acs.org/doi/10.1021/acs.jpcc.2c02396.

Bode plots of the *T*-dependent EIS and EC parameters for all states of charges (PDF)

AUTHOR INFORMATION

Corresponding Author

Burak Ülgüt − *Department of Chemistry, Bilkent University, Ankara 06800, Turkey;* orcid.org/0000-0002-4402-0033; Email: ulgut@fen.bilkent.edu.tr

Authors

Mohammed Ahmed Zabara − *Department of Chemistry, Bilkent University, Ankara 06800, Turkey;* Present Address: Sabancı University, SUNUM, Istanbul, 34956, Turkey; orcid.org/0000-0002-4195-6258

Gökberk Katırcı − *Department of Chemistry, Bilkent University, Ankara 06800, Turkey*

Complete contact information is available at: https://pubs.acs.org/10.1021/acs.jpcc.2c02396

Notes

The authors declare no competing financial interest.

ACKNOWLEDGMENTS

BU would like to acknowledge TÜBA-GEBİP for the young investigator award and BAGEP for the young scientist award.

ADDITIONAL NOTE

[a]In the $Li/SOCl_2$ Nyquist plot, there is a small semicircle following the inductive behavior (between 1 MHz to 100 kHz) which is not *T*-dependent. This semicircle is concluded to be originating from the charge transfer in the current collector, which should be independent of the temperature change. This part of the spectrum will not be analyzed further.

REFERENCES

(1) Aifantis, K. E.; Hackney, S. A.; Kumar, R. V. *High Energy Density Lithium Batteries: Materials, Engineering, Applications*; Wiley-VCH, 2010.

(2) Manthiram, A. An Outlook on Lithium Ion Battery Technology. *ACS Central Science* **2017**, *3*, 1063−1069.
(3) Winter, M.; Barnett, B.; Xu, K. Before Li Ion Batteries. *Chem. Rev.* **2018**, *118*, 11433−11456.
(4) Wood, K. N.; Noked, M.; Dasgupta, N. P. Lithium Metal Anodes: Toward an Improved Understanding of Coupled Morphological, Electrochemical, and Mechanical Behavior. *ACS Energy Lett.* **2017**, *2*, 664−672.
(5) Liu, B.; Zhang, J.-G.; Xu, W. Advancing Lithium Metal Batteries. *Joule* **2018**, *2*, 833−845.
(6) Albertus, P.; Babinec, S.; Litzelman, S.; Newman, A. Status and Challenges in Enabling the Lithium Metal Electrode for High-Energy and Low-Cost Rechargeable Batteries. *Nat. Energy* **2018**, *3*, 16−21.
(7) Hatzell, K. B.; Chen, X. C.; Cobb, C. L.; Dasgupta, N. P.; Dixit, M. B.; Marbella, L. E.; McDowell, M. T.; Mukherjee, P. P.; Verma, A.; Viswanathan, V.; et al. Challenges in Lithium Metal Anodes for Solid-State Batteries. *ACS Energy Lett.* **2020**, *5*, 922−934.
(8) Zhang, S. S. Problem, Status, and Possible Solutions for Lithium Metal Anode of Rechargeable Batteries. *ACS Appl. Energy Mater.* **2018**, *1*, 910−920.
(9) Horstmann, B.; Shi, J.; Amine, R.; Werres, M.; He, X.; Jia, H.; Hausen, F.; Cekic-Laskovic, I.; Wiemers-Meyer, S.; Lopez, J.; Galvez-Aranda, D.; et al. Strategies towards Enabling Lithium Metal in Batteries: Interphases and Electrodes. *Energy Environ. Sci.* **2021**, *14*, 5289−5314.
(10) Fang, C.; Wang, X.; Meng, Y. S. Key Issues Hindering a Practical Lithium-Metal Anode. *Trends Chem.* **2019**, *1*, 152−158.
(11) Xu, W.; Wang, J.; Ding, F.; Chen, X.; Nasybulin, E.; Zhang, Y.; Zhang, J.-G. Lithium Metal Anodes for Rechargeable Batteries. *Energy Environ. Sci.* **2014**, *7*, 513−537.
(12) Liu, H.; Cheng, X. B.; Xu, R.; Zhang, X. Q.; Yan, C.; Huang, J. Q.; Zhang, Q. Plating/Stripping Behavior of Actual Lithium Metal Anode. *Adv. Energy Mater.* **2019**, *9*, 1902254.
(13) Xiao, P.; Luo, R.; Piao, Z.; Li, C.; Wang, J.; Yu, K.; Zhou, G.; Cheng, H.-M. High-Performance Lithium Metal Batteries with a Wide Operating Temperature Range in Carbonate Electrolyte by Manipulating Interfacial Chemistry. *ACS Energy Lett.* **2021**, *6*, 3170−3179.
(14) Wu, C.; Guo, F.; Zhuang, L.; Ai, X.; Zhong, F.; Yang, H.; Qian, J. Mesoporous Silica Reinforced Hybrid Polymer Artificial Layer for High-Energy and Long-Cycling Lithium Metal Batteries. *ACS Energy Lett.* **2020**, *5*, 1644−1652.
(15) Zheng, G.; Wang, C.; Pei, A.; Lopez, J.; Shi, F.; Chen, Z.; Sendek, A. D.; Lee, H.-W.; Lu, Z.; Schneider, H.; et al. High-Performance Lithium Metal Negative Electrode with a Soft and Flowable Polymer Coating. *ACS Energy Lett.* **2016**, *1*, 1247−1255.
(16) Meddings, N.; Heinrich, M.; Overney, F.; Lee, J.-S.; Ruiz, V.; Napolitano, E.; Seitz, S.; Hinds, G.; Raccichini, R.; Gaberšček, M.; Park, J. Application of Electrochemical Impedance Spectroscopy to Commercial Li-Ion Cells: A Review. *J. Power Sources* **2020**, *480*, 228742.
(17) Zhang, Y.; Tang, Q.; Zhang, Y.; Wang, J.; Stimming, U.; Lee, A. A. Identifying Degradation Patterns of Lithium Ion Batteries from Impedance Spectroscopy Using Machine Learning. *Nat. Commun.* **2020**, *11*, 1706.
(18) Habte, B. T.; Jiang, F. Effect of Microstructure Morphology on Li-Ion Battery Graphite Anode Performance: Electrochemical Impedance Spectroscopy Modeling and Analysis. *Solid State Ionics* **2018**, *314*, 81−91.
(19) Zabara, M. A.; Uzundal, C. B.; Ulgut, B. Linear and Nonlinear Electrochemical Impedance Spectroscopy Studies of Li/SOCl 2 Batteries. *J. Electrochem. Soc.* **2019**, *166*, A811−A820.
(20) Zhou, X.; Huang, J.; Pan, Z.; Ouyang, M. Impedance Characterization of Lithium-Ion Batteries Aging under High-Temperature Cycling: Importance of Electrolyte-Phase Diffusion. *J. Power Sources* **2019**, *426*, 216−222.
(21) Stroe, D.-I.; Knap, V.; Swierczynski, M.; Schaltz, E. Electrochemical Impedance Spectroscopy-Based Electric Circuit Modeling of Lithium-Sulfur Batteries during a Discharging State. *IEEE Trans. Ind. Appl.* **2019**, *55*, 631−637.
(22) Zabara, M. A.; Ulgut, B. Electrochemical Impedance Spectroscopy Based Voltage Modeling of Lithium Thionyl Chloride (Li/SOCl2) Primary Battery at Arbitrary Discharge. *Electrochim. Acta* **2020**, *334*, 135584.
(23) Wang, X.; Wei, X.; Dai, H. Estimation of State of Health of Lithium-Ion Batteries Based on Charge Transfer Resistance Considering Different Temperature and State of Charge. *J. Energy Storage* **2019**, *21*, 618−631.
(24) Wang, Z.; Feng, G.; Zhen, D.; Gu, F.; Ball, A. A Review on Online State of Charge and State of Health Estimation for Lithium-Ion Batteries in Electric Vehicles. *Energy Rep.* **2021**, *7*, 5141−5161.
(25) Zappen, H.; Ringbeck, F.; Sauer, D. Application of Time-Resolved Multi-Sine Impedance Spectroscopy for Lithium-Ion Battery Characterization. *Batteries* **2018**, *4*, 64.
(26) Fischer, A.; Kallel, A. Y.; Kanoun, O. Comparative Study of Excitation Signals for Microcontroller-Based EIS Measurement on Li-Ion Batteries. In *2021 International Workshop on Impedance Spectroscopy (IWIS)*; IEEE, 2021; pp 44−47.
(27) Zabara, M. A.; Göçmez, H.; Karabatak, A.; Ulgut, B. Characterization of Different Electrolyte Composition Lithium Thionyl Chloride Reserve Battery by Electrochemical Impedance Spectroscopy. *J. Electrochem. Soc.* **2021**, *168*, 050529.
(28) Li, X.; Zhang, K.; Mitlin, D.; Yang, Z.; Wang, M.; Tang, Y.; Jiang, F.; Du, Y.; Zheng, J. Fundamental Insight into Zr Modification of Li- and Mn-Rich Cathodes: Combined Transmission Electron Microscopy and Electrochemical Impedance Spectroscopy Study. *Chem. Mater.* **2018**, *30*, 2566−2573.
(29) Kitz, P. G.; Lacey, M. J.; Novák, P.; Berg, E. J. Operando EQCM-D with Simultaneous in Situ EIS: New Insights into Interphase Formation in Li Ion Batteries. *Anal. Chem.* **2019**, *91*, 2296−2303.
(30) Li, X.; Guan, H.; Ma, Z.; Liang, M.; Song, D.; Zhang, H.; Shi, X.; Li, C.; Jiao, L.; Zhang, L. In/Ex-Situ Raman Spectra Combined with EIS for Observing Interface Reactions between Ni-Rich Layered Oxide Cathode and Sulfide Electrolyte. *J. Energy Chem.* **2020**, *48*, 195−202.
(31) Ma, S.; Jiang, M.; Tao, P.; Song, C.; Wu, J.; Wang, J.; Deng, T.; Shang, W. Temperature Effect and Thermal Impact in Lithium-Ion Batteries: A Review. *Prog. Nat. Sci.: Mater. Int.* **2018**, *28*, 653−666.
(32) Momma, T.; Matsunaga, M.; Mukoyama, D.; Osaka, T. Ac Impedance Analysis of Lithium Ion Battery under Temperature Control. *J. Power Sources* **2012**, *216*, 304−307.
(33) Erol, S.; Orazem, M. E. The Influence of Anomalous Diffusion on the Impedance Response of LiCoO2|C Batteries. *J. Power Sources* **2015**, *293*, 57−64.
(34) Keefe, A. S.; Buteau, S.; Hill, I. G.; Dahn, J. R. Temperature Dependent EIS Studies Separating Charge Transfer Impedance from Contact Impedance in Lithium-Ion Symmetric Cells. *J. Electrochem. Soc.* **2019**, *166*, A3272−A3279.
(35) Adams, R. A.; Varma, A.; Pol, V. G. Temperature Dependent Electrochemical Performance of Graphite Anodes for K-Ion and Li-Ion Batteries. *J. Power Sources* **2019**, *410*−*411*, 124−131.
(36) Sagane, F.; Abe, T.; Ogumi, Z. Li + -Ion Transfer through the Interface between Li + -Ion Conductive Ceramic Electrolyte and Li + -Ion-Concentrated Propylene Carbonate Solution. *J. Phys. Chem. C* **2009**, *113*, 20135−20138.
(37) Xu, K.; Von Cresce, A.; Lee, U. Differentiating Contributions to "Ion Transfer" Barrier from Interphasial Resistance and Li+ Desolvation at Electrolyte/Graphite Interface. *Langmuir* **2010**, *26*, 11538−11543.
(38) Shi, S.; Lu, P.; Liu, Z.; Qi, Y.; Hector, L. G.; Li, H.; Harris, S. J. Direct Calculation of Li-Ion Transport in the Solid Electrolyte Interphase. *J. Am. Chem. Soc.* **2012**, *134*, 15476−15487.
(39) Jow, T. R.; Delp, S. A.; Allen, J. L.; Jones, J.-P.; Smart, M. C. Factors Limiting Li + Charge Transfer Kinetics in Li-Ion Batteries. *J. Electrochem. Soc.* **2018**, *165*, A361−A367.

https://doi.org/10.1021/acs.jpcc.2c02396
J. Phys. Chem. C 2022, 126, 10968−10976

(40) Li, Y.; Leung, K.; Qi, Y. Computational Exploration of the Li-Electrode|Electrolyte Interface in the Presence of a Nanometer Thick Solid-Electrolyte Interphase Layer. *Acc. Chem. Res.* **2016**, *49*, 2363−2370.
(41) Wang, A.; Kadam, S.; Li, H.; Shi, S.; Qi, Y. Review on Modeling of the Anode Solid Electrolyte Interphase (SEI) for Lithium-Ion Batteries. *npj Comput. Mater.* **2018**, *4*, 15.
(42) Yamada, Y.; Iriyama, Y.; Abe, T.; Ogumi, Z. Kinetics of Lithium Ion Transfer at the Interface between Graphite and Liquid Electrolytes: Effects of Solvent and Surface Film. *Langmuir* **2009**, *25*, 12766−12770.
(43) Xu, K. Charge-Transfer" Process at Graphite/Electrolyte Interface and the Solvation Sheath Structure of Li[Sup +] in Nonaqueous Electrolytes. *J. Electrochem. Soc.* **2007**, *154*, A162.
(44) Yamada, Y.; Sagane, F.; Iriyama, Y.; Abe, T.; Ogumi, Z. Kinetics of Lithium-Ion Transfer at the Interface between Li 0.35La0.55TiO3 and Binary Electrolytes. *J. Phys. Chem. C* **2009**, *113*, 14528−14532.
(45) Xu, K.; Lam, Y.; Zhang, S. S.; Jow, T. R.; Curtis, T. B. Solvation Sheath of Li+ in Nonaqueous Electrolytes and Its Implication of Graphite/Electrolyte Interface Chemistry. *J. Phys. Chem. C* **2007**, *111*, 7411−7421.
(46) Single, F.; Horstmann, B.; Latz, A. Theory of Impedance Spectroscopy for Lithium Batteries. *J. Phys. Chem. C* **2019**, *123*, 27327.
(47) Huang, J.; Gao, Y.; Luo, J.; Wang, S.; Li, C.; Chen, S.; Zhang, J. Editors' Choice-Review-Impedance Response of Porous Electrodes: Theoretical Framework, Physical Models and Applications. *J. Electrochem. Soc.* **2020**, *167*, 166503.
(48) Dai, J.; Yang, C.; Wang, C.; Pastel, G.; Hu, L.; Dai, J.; Yang, C.; Wang, C.; Pastel, G.; Hu, L. Interface Engineering for Garnet-Based Solid-State Lithium-Metal Batteries: Materials, Structures, and Characterization. *Adv. Mater.* **2018**, *30*, 1802068.
(49) Xia, J.; Madec, L.; Ma, L.; Ellis, L. D.; Qiu, W.; Nelson, K. J.; Lu, Z.; Dahn, J. R. Study of Triallyl Phosphate as an Electrolyte Additive for High Voltage Lithium-Ion Cells. *J. Power Sources* **2015**, *295*, 203−211.
(50) Orazem, M. E.; Esteban, J. M.; Moghissi, O. C. Practical Applications of the Kramers-Kronig Relations. *Corrosion* **1991**, *47*, 248−259.
(51) Boukamp, B. A. A Linear Kronig-Kramers Transform Test for Immittance Data Validation. *J. Electrochem. Soc.* **1995**, *142*, 1885.
(52) Levi, M. D.; Wang, C.; Markevich, E.; Aurbach, D.; Chvoj, Z. Noteworthy Electroanalytical Features of the Stage 4 to Stage 3 Phase Transition in Lithiated Graphite. *J. Solid State Electrochem.* **2003**, *8*, 40−43.
(53) Levi, M. D.; Wang, C.; Aurbach, D.; Chvoj, Z. Effect of Temperature on the Kinetics and Thermodynamics of Electrochemical Insertion of Li-Ions into a Graphite Electrode. *J. Electroanal. Chem.* **2004**, *562*, 187−203.
(54) Chang, W.; Bommier, C.; Mohr, R.; Steingart, D. Impact of Non-Arrhenius Temperature Behavior on the Fast-Charging Capabilities of LiCoO2-Graphite Lithium-Ion Batteries. *J. Phys. Chem. C* **2021**, *125*, 1731.
(55) Heins, T. P.; Harms, N.; Schramm, L.-S.; Schröder, U. Development of a New Electrochemical Impedance Spectroscopy Approach for Monitoring the Solid Electrolyte Interphase Formation. *Energy Technol.* **2016**, *4*, 1509−1513.
(56) Ishikawa, H.; Nishikawa, Y.; Umeda, M. Comparison of Activation Energies of Laminated Lithium-Ion Secondary Cell Using LiCoO2 and LiMn2O4 as Cathode Material by AC Impedance Method. *J. Renew. Sustain. Energy* **2011**, *3*, 053106.
(57) Li, J.; Yuan, C. F.; Guo, Z. H.; Zhang, Z. A.; Lai, Y. Q.; Liu, J. Limiting Factors for Low-Temperature Performance of Electrolytes in LiFePO 4/Li and Graphite/Li Half Cells. *Electrochim. Acta* **2012**, *59*, 69−74.
(58) Wu, H.; Jia, H.; Wang, C.; Zhang, J. G.; Xu, W.; Wu, H.; Jia, H.; Zhang, J.-G.; Xu, W.; Wang, C. Recent Progress in Understanding Solid Electrolyte Interphase on Lithium Metal Anodes. *Adv. Energy Mater.* **2021**, *11*, 2003092.
(59) Horstmann, B.; Single, F.; Latz, A. Review on Multi-Scale Models of Solid-Electrolyte Interphase Formation. *Curr. Opin. Electrochem.* **2019**, *13*, 61−69.
(60) Montesperelli, G. Li Passivation in Different Electrolytes during Storage and Cycling — An Impedance Spectroscopy Study. *Solid State Ionics* **1990**, *37*, 149−156.
(61) Leef, A.; Gilmour, A. Voltage Delay in Lithium Non-Aqueous Battery Systems. *J. Appl. Electrochem.* **1979**, *9*, 663−669.
(62) Moshtev, R. V.; Geronov, Y.; Puresheva, B. The Primary Passive Film on Li in SOCl2 Electrolyte Solutions. *J. Electrochem. Soc.* **1981**, *128*, 1851.
(63) Meitav, A.; Peled, E. Solid Electrolyte Interphase (SEI) Electrode. *J. Electroanal. Chem. Interfacial Electrochem.* **1982**, *134*, 49−63.

https://doi.org/10.1021/acs.jpcc.2c02396
J. Phys. Chem. C 2022, 126, 10968−10976